Fabrication of Thermoelectric Conversion Devices Using Porous Si

(多孔質 Si を用いた熱電変換デバイスの作製)

Ibaraki University
Graduate School of Science and Engineering
Major in Quantum Beam Science

18ND108H

Yasutaka Hashimoto

Abstract

Thermoelectric materials have an excellent ability to convert thermal energy to electrical energy and vice versa. Noting that more than 60% of the energy produced in the world is disposed of without being used as waste heat, in recent years, expectations for thermoelectric conversion used as a waste heat recovery technology or an energy acquisition technology from unused heat have been glowing. Silicon (Si) is non-toxic and can behave as P-type or N-type semiconductor by adding a small amount of impurity element. Si has tended to be left out of candidates of materials for thermoelectric conversion modules due to its high thermal conductivity so far. However, because of its abundance and nontoxicity, it is attracting much attention for thermoelectric use for the future society. Recent studies have shown that effective heat transfer coefficient can be improved by making Si porous to compensate

for the disadvantage of high thermal conductivity, and hence use of Si as thermoelectric material could be realized in the not too distant future. Therefore, it is necessary to prepare data for the use of porous Si in thermoelectric devices. There are three major challenges in the fabrication of porous Si devices: fabrication of porous Si, the bonding of Si to metal electrodes, and device design. In this paper, we conducted investigations for the fabrication of devices using porous Si.

First, fabrication of porous Si and Si-B by unidirectional solidification under hydrogen atmosphere was conducted. In this technique, discontinuous decrease in the solubility of hydrogen at the freezing point is utilized for the formation of hydrogen pores elongated unidirectionally in the direction of solidification. The porosity and the average diameter of the prepared sample were evaluated by image-J analysis following observation with optical microscope. And for Si, the influence of doping elements for tuning carrier concentration on the pore formation and the influence of hydrogen dissolved in the Si crystal on the electric properties were examined. As a result, it was found that porous Si-B with unidirectional pores can be produced by unidirectional solidification under a hydrogen atmosphere. The average diameter of pores becomes larger and the porosity increases with the distance from the cooling surface. There is no significant difference between Si and Si-B in porosity and average diameter. It is also found that the effect of B-doping on pore formation is not significant. Regarding electrical properties, first of all, it was found that the carrier concentration of porous Si doped with B, which contains hydrogen atoms as solutes, is significantly higher than non-doped Si. That is, B, which is often used as a dopant for Si for tuning carrier concentration, works as a dopant in porous Si as well. On the other hand, the measured carrier concentration in the B-doped sample tends to scatter. This is due to the segregation of B. Furthermore, it was confirmed that

the residual hydrogen in porous Si and Si-B can be decreased by annealing process with vacuum evacuation. Regarding the relationship between electrical conductivity and porosity, the electrical conductivity decreases in the direction perpendicular to the porosity as the porosity increases.

Second, the bonding conditions of porous thermoelectric material and metal electrodes are examined. In order to fabricate thermoelectric conversion devices, the bonding of thermoelectric material and metal electrode is essential. In particular, silver (Ag) is one of candidates for metal electrodes because of its high electrical conductivity and the absence of intermediate compounds with Si. The bonding properties between Si and Ag at the atomic scale and the shear strength have been reported in the past. However, more data such as bonding strength and contact resistance are needed for fabrication of thermoelectric devices using porous Si and their use. The present study investigates the diffusion bonding between Si and Ag. The bonding strength and interfacial electrical resistivity have been evaluated. Bonding between Si and Ag were executed using a diffusion bonding technique. Diffusion bonding was performed under a uniaxial pressure at a high temperature in an Ar atmosphere with various pressures for various periods. The bonding strength was measured with a tensile tester. The electrical resistances of bonded samples were measured using a thermoelectric measurement and evaluation system. As a result, the diffusion bonding was successfully made at 1103 K under unidirectional compression load. No intermediate phase was observed consistently with the reported Ag-Si equilibrium phase diagram. The bonding strength increases with increasing bonding time up to 90 min while it does not vary around 8 MPa with bonding time longer than 90 min for the bonding with a 20 MPa bonding pressure followed by slow cooling. Furthermore, the diffusion bonding between Ag and Si was found to satisfy the bonding strength required for thermoelectric devices using porous Si. The interfacial electrical resistivity is in the order of 10^{-10} Ωm^2 and there is no significant variation with bonding time. Thus, Ag is useful as metallic electrodes for Si.

Finally, porous Si devices were fabricated. In this porous thermoelectric conversion device, the thermal fluid flows through pores of the thermoelectric materials and exchanges heat. Increase in thermal interface is the greatest advantage. Alternately arranging porous Si-B (P-type) and Si-Sb (N-type) connected with the electrodes in between and thermal insulation material, the flow paths are formed in a direction perpendicular to the plate. High-/low-temperature fluids alternately flows in the path and causes the thermal electromotive force. Hand-drilled Si wafers were used as the porous Si (diameter 1.2 mm, porosity 9.38 %). The devices were fabricated in a size of 17 mm × 17 mm, with one Si-B and one Si-Sb bonded to each other with Ag. Hot (about 353 K)

and cold (about 293 K) temperature fluids flowed through the device, and electrical voltages of an order of mV were obtained.

Table of contents

1. Introduction

Global environmental problems such as the depletion of fossil fuels and other resources have attracted much attentions. Therefore, measures have been taken for reduction of energy consumption and use of renewable energies. Thermoelectric materials have an excellent ability to convert thermal energy to electrical energy and vice versa. Noting that more than 60% of the energy produced in the world is disposed of without being used as waste heat, in recent years, expectations for thermoelectric conversion as a waste heat recovery technology or an energy acquisition technology from unused heat have been glowing [1)]. In addition, when the highly IoT-oriented human society described in Society 5.0 is realized, a trillion sensors of all kinds are expected to acquire various kinds of data and AI will analyze them. in order to operate huge number of sensors, there are high expectations for thermoelectric conversion technology, which can be used as maintenance-free and independent power sources [2)]. For these reasons, there is an urgent need to develop thermoelectric conversion devices that can be mass-produced at low cost, have high efficiency, and do not contain harmful elements.

We focused on porous Si as a material that could satisfy these requirements and tried to fabricate devices. There are three major challenges in the fabrication of porous Si devices: fabrication of porous Si, the bonding of Si to metal electrodes, and device design. In this paper, we conducted investigations for the fabrication of devices using porous Si. Background and purpose of this study was introduced in Chapter 1, and the fabrication of porous Si as thermoelectric material in Chapter 2, and bonding of Si to metal electrodes in Chapter 3, and device design in Chapter 4 was discussed.

1-1. Thermoelectric effect

The thermoelectric effect can be classified into Seebeck effect, Peltier effect and Thomson effect. The Seebeck effect is a phenomenon in which an electromotive force is generated when two different metals or semiconductors are joined, and a temperature difference is applied to both ends. In thermoelectric power generation, this effect is used to convert thermal energy into electrical energy. The Peltier effect is a phenomenon in which heat or endothermy is generated when an electric current is passed through a contact surface. The Thomson effect is the effect of heat absorption or generation when an electric current is passed between two points with a temperature difference on a metal.

Thermoelectric power generation devices have the advantages of being maintenance-free, easy to miniaturize, and emit no carbon dioxide or other gases because they do not have an operating part. Since thermoelectric materials can convert the thermal energy of waste heat into electrical energy, thermoelectric materials are expected to be a new energy source. However, this power generation method has been used in limited situations such as power sources for space probes and small refrigerators because of its low energy conversion efficiency compared to other power generation methods, and it is not widely used. Therefore, it is necessary to address the issues of improving the properties and conversion efficiency of thermoelectric conversion materials for the practical application and spread of large-scale thermoelectric power generation systems. The maximum efficiency of thermoelectric conversion, η_{max}, is given by

$$\eta_{max} = \frac{\Delta T}{T_h} \cdot \frac{M-1}{M + T_c/T_h}, \qquad (1)$$

where $\Delta T (= T_h - T_c)$ is the temperature difference in the thermoelectric element, $\Delta T/T_h$ is the Carnot efficiency, and M is defined as $(1+zT)^{1/2}$. The figure of merit zT is a value to compare the thermoelectric quality of different materials[3]. The conversion efficiency depends on zT, and the improvement of zT increases the conversion efficiency. figure of merit, zT, given by

$$zT = \frac{S^2\sigma}{\kappa} T \propto m^{*\frac{3}{2}} \left(\frac{\mu}{\kappa_L}\right) T, \qquad (2)$$

where S is the Seebeck coefficient, σ is the electrical conductivity and κ is the thermal conductivity, κ_L is the lattice thermal conductivity, m is the effective mass of holes or electrons, and μ is the mobility. From formula (1)(2), decreasing the lattice thermal conductivity while maintaining the high electrical conductivity leads to an increase in the maximum conversion efficiency η_{max}. Even if the thermal conductivity is high, the temperature difference can be large by making the device longer, but the energy loss is caused by Joule heat generation due to the electrical resistance of the device itself. Thus, a device material with low thermal conductivity is required. For this reason, research has been conducted to reduce the lattice thermal conductivity and improve the power factor ($S^2\sigma$) of thermoelectric materials.

1-2. Toward higher thermoelectric conversion efficiency

In general, a lot of research has been done to improve zT in order to improve the thermoelectric conversion efficiency. On the other hand, there is a method to obtain more thermoelectromotive force by promoting heat transfer between thermoelectric material and heat source fluid. In this study, thermoelectric devices were fabricated by using porous thermoelectric materials in order to increase the specific surface area and the effective heat transfer coefficient (Fig. 1-1). The objective of this work is to generate highly efficient power by promoting the heat transfer between the heat source fluid and the device. Power generation devices based on porous thermoelectric materials have been published in previous studies[4]. This device is a device in which combustion gas flows into a power generating device and a large temperature difference is obtained by combustion[5]. Applying this idea, we have devised a new fluid-permeable thermoelectric device. A schematic diagram is shown in Fig. 1-2.

The temperature distribution and heat flow in a general π-type thermoelectric device are shown in Fig. 1-3. The maximum temperature difference that a module can take (temperature difference between the heat source fluid) is defined as ΔT_0, the temperature difference in the thermoelectric device is defined as ΔT_1, the temperature difference between the heat source fluid and the thermoelectric device is defined as $\Delta(T_0 - T_1)$, and the length of the thermoelectric device is defined as d. Heat transfer between the heat source fluid and the thermoelectric device is done by heat transfer. The heat flux J_Q, is given by

$$J_Q = h\Delta(T_0 - T_1) \qquad (3)$$

where h is the heat transfer coefficient. The heat transfer coefficient is a value that indicates the ease of heat energy transfer through the interface between two materials and is the heat flux density per unit temperature difference ($W/m^2 K$).

In addition, assuming a constant temperature gradient and ignoring the energy flowing into the element due to Peltier effect and Joule heat, the heat flow J_Q in the element is given by

$$J_Q = -\kappa \frac{\Delta T_1}{d} \qquad (4)$$

where κ is the thermal conductivity. Assuming that the heat flow is equal, the following equations are obtained from (3) and (4).

$$J_Q = \Delta T_0 \left(\frac{1}{\frac{1}{h} + \frac{d}{\kappa}} \right) \quad (5)$$

$$\frac{\Delta T_1}{\Delta T_0} = \frac{1}{1 + \frac{\kappa}{hd}} \quad (6)$$

Equation (5) shows the relationship between the temperature difference between the heat source fluid and the heat flow, and Equation (6) shows the relationship between the temperature difference between the heat source fluid and the temperature difference in the device. From equation (5), it is necessary to reduce d/ κ or 1/ h to increase the heat flow J_Q. However, as the thermal conductivity k is increased, the conversion efficiency zT of equation (2) becomes smaller, and the heat flowing into the device increases, but the amount of heat converted into electrical energy in the device decreases, so increasing k is not desirable. Therefore, it is desirable to reduce 1/ h (increase the heat transfer coefficient). Similarly, from equation (6), it can be said that a large h is significant in terms of improvement in conversion efficiency. Equation (6) expresses how close the temperature difference in the device can be to the temperature difference between the heat source fluids, and It affects the electromotive force. The left side of equation (6) is the ratio of the temperature difference in the thermoelectric device to the maximum temperature difference available for power generation. The closer this ratio is to 1, the more temperature difference between the heat source fluids can be incorporated into the power generation, the greater voltage was obtained. In other words, by increasing the heat transfer coefficient h, a large voltage can be obtained. In addition, considering a certain ratio, the length d of the thermoelectric device giving the same electromotive force can be shortened. Therefore, a reduction in electrical resistance can be expected due to the miniaturization of the device. Moreover, since the effect of thermal conductivity on the thermal electromotive force is diminished, even thermoelectric materials with a large thermal conductivity can be used as an alternative to thermoelectric materials. Thus, it increases the possibility of selection for device use. In summary, the improvement of effective heat transfer coefficient by the porousness of thermoelectric materials can

improve the power generation efficiency of thermoelectric devices. It is considered to be effective in improving the performance of the system.

1-3. Lotus-type porous material

In fabricating porous thermoelectric conversion devices, the requirements for porous materials include excellent thermoelectric properties (especially $S^2\sigma$), large pore specific surface area, having through pores, and excellent mechanical properties. Among the porous materials, lotus-type porous materials, in which the pores extend in one direction, are expected to be the materials that satisfy these requirements.

When the metal is melted in a hydrogen atmosphere and then solidified, hydrogen atoms, which cannot be dissolved in the solid phase are deposited as the pores. The porous metal is obtained by the formation of when the solidification direction is controlled in one direction [6], the pores formed grow parallel to the solidification direction. Such a porous metal with unidirectional pores is called a lotus-type porous metal. This lotus-type porous metal has a large surface area and mechanical strength and fluid permeability.

Utilizing these characteristics, it has been put into practical use as heat sinks for devices and have higher heat transfer performance than conventional heat sinks [7, 8]. If this lotus-type porous thermoelectric material can be applied to thermoelectric devices, it is expected to create new power generation devices with higher thermoelectric conversion efficiency than the conventional ones. For application in devices, it is necessary to investigate the properties of porous thermoelectric materials as thermoelectric materials.

1-4. Porous silicon

In terms of environmental issues and IOT, there is an urgent need to develop thermoelectric conversion devices that can be mass-produced at low cost, have high efficiency, and do not contain harmful elements.

Silicon (Si) is non-toxic and can behave as p-type or n-type semiconductor by adding a small amount of impurity element. In addition, Si can be made porous by solidification in hydrogen atmosphere utilizing the solubility gap between liquid and solid states [9]. Si has tended to be left out of candidates of materials for thermoelectric conversion modules due to its high thermal conductivity so far. However, due to its abundance and nontoxicity, it is attracting much attention for thermoelectric use for the future society. Recent studies have shown that nanostructuring is effective for lowering thermal conductivity [10] or the effective heat transfer coefficient can be improved by making Si porous to compensate for the disadvantage of high thermal conductivity [11], hence use of Si as thermoelectric material could be realized in the not too distant future. Therefore, it is necessary to prepare data for the use of porous Si in thermoelectric devices.

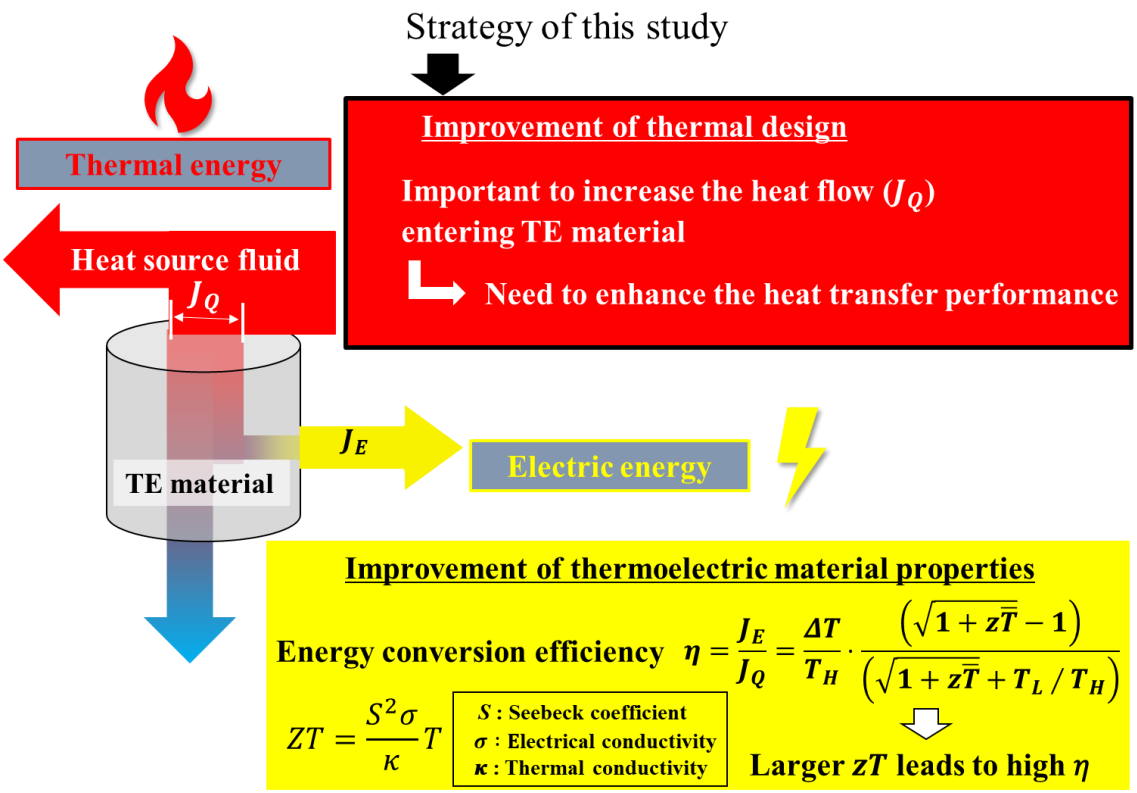

Fig.1-1. Strategies for improving device performance.

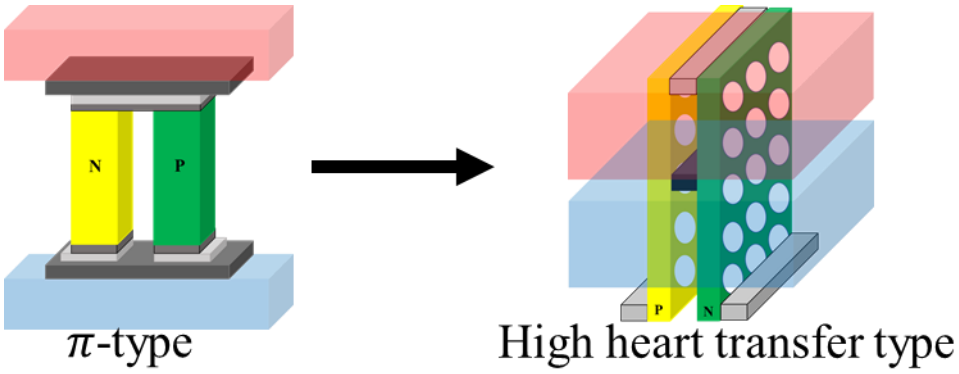

Fig. 1-2. Image of a porous thermoelectric conversion device.

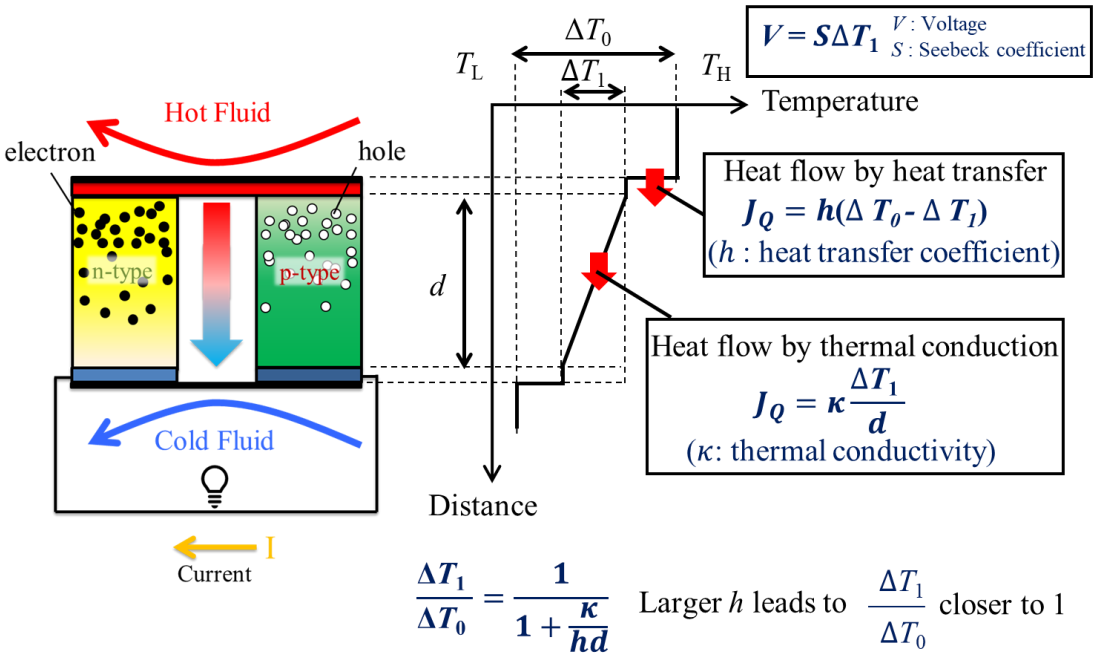

Fig. 1-3. Temperature distribution and heat flow in a general π-type thermoelectric device.

2. Fabrication of porous Si as thermoelectric material

Toward to the fabrication of porous Si as thermoelectric material, the boron (B) doped porous Si was fabricated and its properties were evaluated. In addition, it is considered that there is hydrogen dissolved in the porous Si, and it may affect the thermoelectric properties. Porous Si was annealed for dehydrogenation, and the solid hydrogen concentration in the porous Si and its effect on the electrical properties have been investigated.

2-1. Experimental procedure

2-1-1. Fabrication of Porous Si by Mold Casting Method

In metals that there is a solubility difference between the liquid phase and the solid phase at the melting point, the gas which is not fully dissolved at the time of solidification becomes pores, and porous metal can be fabricated. Porous thermoelectric materials with aligned pores in one direction were fabricated by mold casting method that same way as the method used to fabricate Nakahata's Lotus-type porous Si [9]. The configuration of the equipment chamber in which the mold casting method were conducted is shown in Fig. 2-1. The melting part and solidification part are set up in pressurized gas chamber. After filling raw metallic materials into a crucible, the metals are melted by high-frequency induction heating, in which gas (Ar/H_2) is dissolved under a given atmospheric pressure. The melt is poured into a copper-made mold whose bottom is cooled by a chiller and is solidified unidirectionally from the bottom upward. Thus, the elongated pores grow in the direction of solidification.

Boron was selected as a doped element in Si, and the composition of Si-0.5, 1at.%B were investigated. Si (99.999%pure) and B (99%pure) were placed in an alumina tanman tube (inner diameter: 35 mm, material: SSA-S Nikkato). The samples were melted at 1560°C by an induction heating coil under a constant pressure gas atmosphere (Ar ~0.3 MPa /H_2 ~0.3 MPa) and kept at 1560°C for 10 minutes.

The molten samples were cast into molds with an inner diameter of 30 mm, which were placed on a cooled copper chiller. The molybdenum sheet with a thickness of 0.1 mm was used as the mold. The inside of the mold was coated with a mold release agent (alumina: sodium silicate = 1:1) and allowed to dry. Because the heat capacity of the molybdenum sheet is smaller than that of the copper chiller, the heat dissipation from the sides is less. Therefore, the molten sample solidifies in one direction, from the bottom to the top. The fabricated porous Si ingots were cut perpendicular to the solidification direction at a position 4,8,12,16 mm from the cooling surface by a low-speed cutter for observation and

measurement.

2-1-2. Measurement of carrier concentration and electrical conductivity by Hall effect measurements.

The carrier concentration and electrical conductivity of porous Si and Si-1at.%B samples were evaluated by Hall effect measurements. A sample was cut from a plane perpendicular to the solidification direction at a height of 4 mm from the cooling surface to a size of 5 × 5 mm square and mechanically polished with a diamond slurry (particle size 9 μm) to a thickness of 500 μm. The four corners of the sample and the measurement terminals were then soldered with indium (99.99% pure). The Hall effect measurements were performed by the four-terminal Van Der Pauw method[12] with a magnetic field of 3500 G and a current of 1 mA. The porosity of each sample ε[%] for which the Hall effect was measured was calculated from the density ρ_1 of the measured sample and the density ρ_0 of the bulk Si using the formula (1).

$$\varepsilon = \left[1 - \frac{\rho_1}{\rho_0}\right] \times 100 \qquad (1)$$

Cross-sectional photographs were observed by optical microscopy, and the average diameter of the cross-sectional pore size was determined by image analysis software (Image J ver.1.45 I, National Institutes of Health and the Laboratory for Optical and Computational Instrumentation).

2-1-3. Dehydrogenation by annealing

In the present study, Si was made porous using high-pressure hydrogen gas. Therefore, the presence of residual hydrogen in the porous Si prepared by this method may affect the thermoelectric properties. Hence, the effects of annealing in the porous Si with vacuum evacuation on the concentration of hydrogen and electrical properties were investigated. For the annealing process, a high-temperature atmospheric furnace (FT-01VAC, Flutech) was used, and the furnace was held at 1000°C for 24 hours with vacuum exhausted. The concentration of soluble hydrogen in each sample was measured by the NDIR method using an oxygen/nitrogen/hydrogen quantitative analyzer (EMGA-930, HORIBA).

The electrical characteristics of vacuum-annealed and non-annealed samples were evaluated by Hall effect measurements. For the measurement, a 5 mm×5 mm square section was cut from the surface perpendicular to the solidification direction at 4 mm height from the cooling surface, and the sample was mechanically polished with a diamond slurry liquid to a thickness of 500 μm. After that, the four corners of the sample

and the measurement terminals were soldered with In (99.99% pure), and the sample was subjected to the Hall effect measurement by the DC four-terminal Van der Pauw method under a magnetic field of 3500 G and a current value of 1 mA.

2-2. Results and discussions

2-2-1. Fabrication of Porous Si-B

A cross section of the fabricated porous samples cut parallel/vertical to the solidification direction is shown in Fig. 2-2. In both Si and Si-B samples, the pores are circular in the vertical cross section and the pores are extended in the parallel cross section in the solidification direction. Therefore, it was confirmed that porous Si-B with unidirectional pores can be produced (especially cooling surface~4mm) by unidirectional solidification under a hydrogen atmosphere.

The relationship between the distance from the cooling surface and the average diameter of the pores is shown in Fig. 2-3 (a). The relationship between the distance from the cooling surface and the porosity is shown in Fig. 2-3(b).

Overall, the average diameter of pores becomes larger and the porosity increases with the distance from the cooling surface. It is considered that the pores become larger as the distance from the cooling surface increases, because the cooling effect becomes weaker and the velocity of movement at the solid-liquid interface becomes slower. In the Si-B sample, the porosity decreased from about 12 mm. It is considered that the porosity was decreased due to the escape of hydrogen gas to the upper part of the liquid phase during the formation of the pores. In case of slow movement of the solid-liquid interface, the gas atoms enriched in the liquid phase diffuse over a long distance due to a sufficient diffusion time, the gas atoms reach the pores from farther away, and the pores grow and become coarsened. For this reason, we focus on the average diameter and porosity of 4 mm from the cooling surface, which are less coarsened. There is no significant difference between the diameters of Si and Si-B at 4 mm from the cooling surface. There is no significant difference between Si and Si-B in porosity and average diameter. Thus, it is clear that the effect of B-doping on unidirectional pore formation is small. However, after 8 mm diameter and 12 mm porosity, there is a difference in values between Si and Si-B. This difference should be investigated in detail in the future.

2-2-2. Effect of Porosity on Electrical Conductivity

Regarding the electrical conductivity of porous materials, it has been reported that the electrical conductivity of lotus-type porous metals decreases with the increase in porosity. The reason for this is that the current carrier in the sample moves around the pores, which increases the travel distance and the electrical resistivity.

The relationship between the electrical conductivity and porosity of porous Si-0.5at. %B perpendicular to the pores are shown in Fig. 2-3. As the porosity increased, the electrical conductivity of porous Si perpendicular to the pores are decreased. This result is

qualitatively similar to the trend for the Lotus nickel. however, it is confirmed that there is more variability in the Si plots than in the nickel plots. This is thought to be due to differences in electrical conductivity and ductility. In terms of electrical conductivity, the electrical conduction in nickel is caused by the transfer of free electrons. On the other hand, the bias of the dopant distribution in the sample changes the value of the electrical conductivity of Si, because the electrical conductivity is controlled by the dopant addition. Therefore, in order to discuss the porosity dependence of electrical conductivity in lotus Si, it is essential to control the carrier concentration in porous Si uniformly. In addition, Nickel has high ductility and malleability. In contrast, Si is harder and more brittle than nickel. Therefore, cracks may occur in the Si during unidirectional solidification or when cutting out the sample. Since cracks can reduce carrier mobility as well as pores, it is necessary to suppress cracks in order to study the dependence of electrical properties on pores.

2-2-3. Effect of residual hydrogen on Electrical Properties

The results of the Hall effect measurements of Si-1at. %B and Si are shown in Table. 2-1. The difference in carrier concentration confirms that the samples are doped. There was no significant difference in the Si samples due to residual hydrogen.

On the other hand, the carrier concentration in the B-doped sample varied with the presence or absence of hydrogen solid solution. Hence, the same sample was cut at 4 mm intervals from the cooling surface, and Hall effect measurements were performed for each sample. The results are shown in Table. 2-2. It was found that the carrier concentration varied within the sample, suggesting that B segregation occurred in the sample.

Therefore, the difference in the carrier concentration in the B-doped samples is inferred to be due to the segregation of B, it is considered that the effect of residual hydrogen on the electrical properties is small. However, no trend in the relationship between the cooling surface and segregation could be confirmed, so the samples must be cut at a narrower interval for further investigation.

2-2-4. Effects of dehydrogenation by annealing

The relationship between the concentration of soluble hydrogen and electrical conductivity of porous Si-B and porous Si before / after annealing are shown in Fig. 2-4. It was confirmed that the concentration of soluble hydrogen in porous Si-B and porous Si after annealing was lower than that in the before annealing sample. It proved that the dehydrogenation of porous Si was found to be possible by the annealing process with vacuum evacuation. Since the electrical conductivity of both samples did not change

significantly before and after annealing, the effect of the residual hydrogen on the electrical properties of the porous Si is small. In other words, it is possible to prevent hydrogen embrittlement without affecting the electrical properties by annealing.

The Hall effect measurements of porous Si before and after annealing with vacuum evacuation are shown in Table 2-3. The carrier concentration decreased, and the mobility increased in the porous Si after annealing. This is thought to be due to the recovery of crystals by annealing.

2-3 Conclusions

This chapter studied the properties of porous b-doped Si that fabricated by mold casting method. It was confirmed that porous Si-B with unidirectional pores can be produced by unidirectional solidification under a hydrogen atmosphere. The average diameter of pores becomes larger and the porosity increases with the distance from the cooling surface. There is no significant difference between Si and Si-B in porosity and average diameter. It is also found that the effect of B-doping on pore formation is not significant. Regarding electrical properties, first of all, it was found that the carrier concentration of porous Si doped with B, which contains hydrogen atoms as solutes, is significantly higher than non-doped Si. That is, B, which is often used as a dopant for Si for tuning carrier concentration, works as a dopant in porous Si as well. On the other hand, the measured carrier concentration in the B-doped sample tends to scatter. This is due to the segregation of B. Regarding the relationship between electrical conductivity and porosity, the electrical conductivity decreases in the direction perpendicular to the porosity as the porosity increases. Furthermore, it was confirmed that the residual hydrogen in porous Si and Si-B can be decreased by annealing process with vacuum evacuation.

Table. 2-1. Differences in carrier concentration by presence/absence of hydrogen solid solution and B-doped.

	Non-hydrogen solid solution (Ar 0.3 [MPa])	Hydrogen solid solution (H_2 0.3 [MPa])
Si [cm^{-3}]	1.3×10^{18}	4.7×10^{18}
Si-1at.%B [cm^{-3}]	1.5×10^{21}	1.4×10^{20}

Table. 2-2. Carrier concentration in the sample (H_2 0.3 [MPa]).

Distance from the cooling surface [mm]	Carrier concentration [cm^{-3}]
4	5.2×10^{20}
8	8.2×10^{21}
12	1.5×10^{21}
16	3.0×10^{20}

Table. 2-3. Electrical properties of porous Si before and after annealing.

	Resistivity [$10^{-4}\Omega\cdot$cm]	Carrier concentration [cm-3]	Mobility [$cm^2/V\cdot sec$]
As-cast Si-0.5at.%B	7.2	3.9×10^{20}	2.2×10^{1}
Annealed Si-0.5at.%B	6.7	7.3×10^{19}	1.3×10^{2}

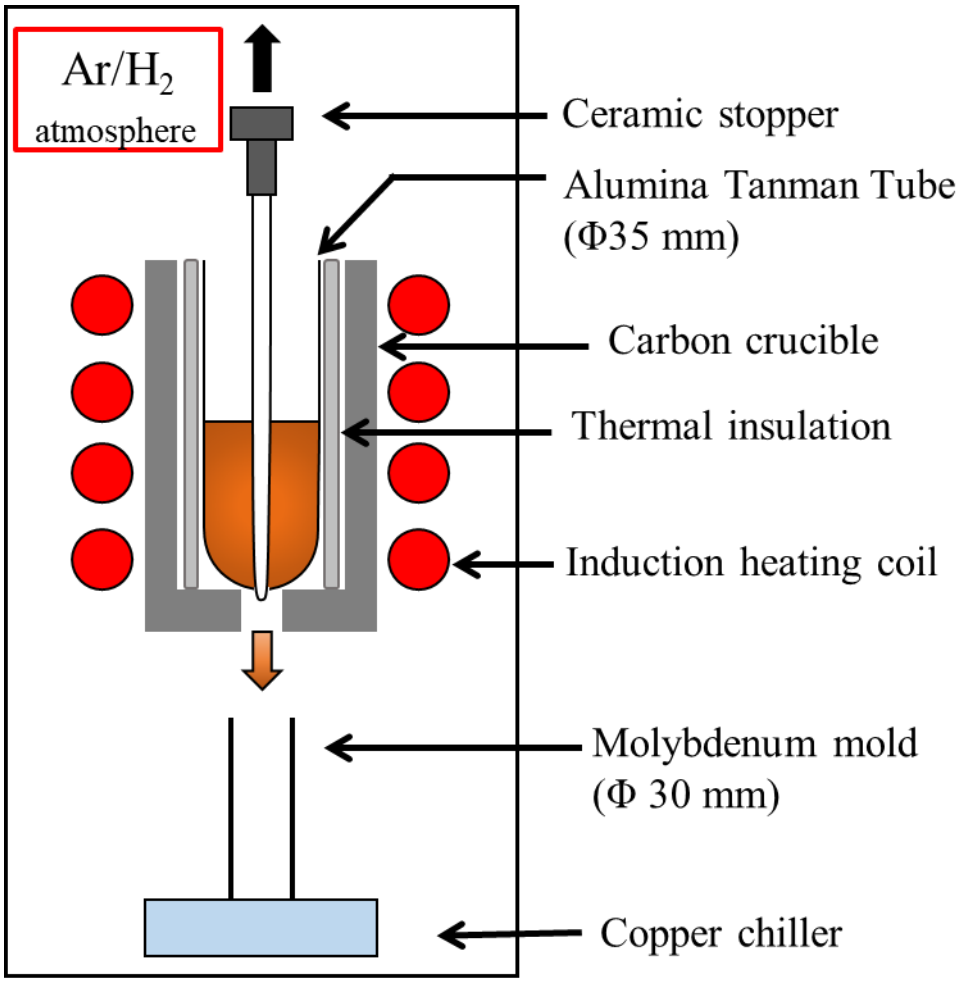

Fig. 2-1. Schematic diagram of mold casting method.

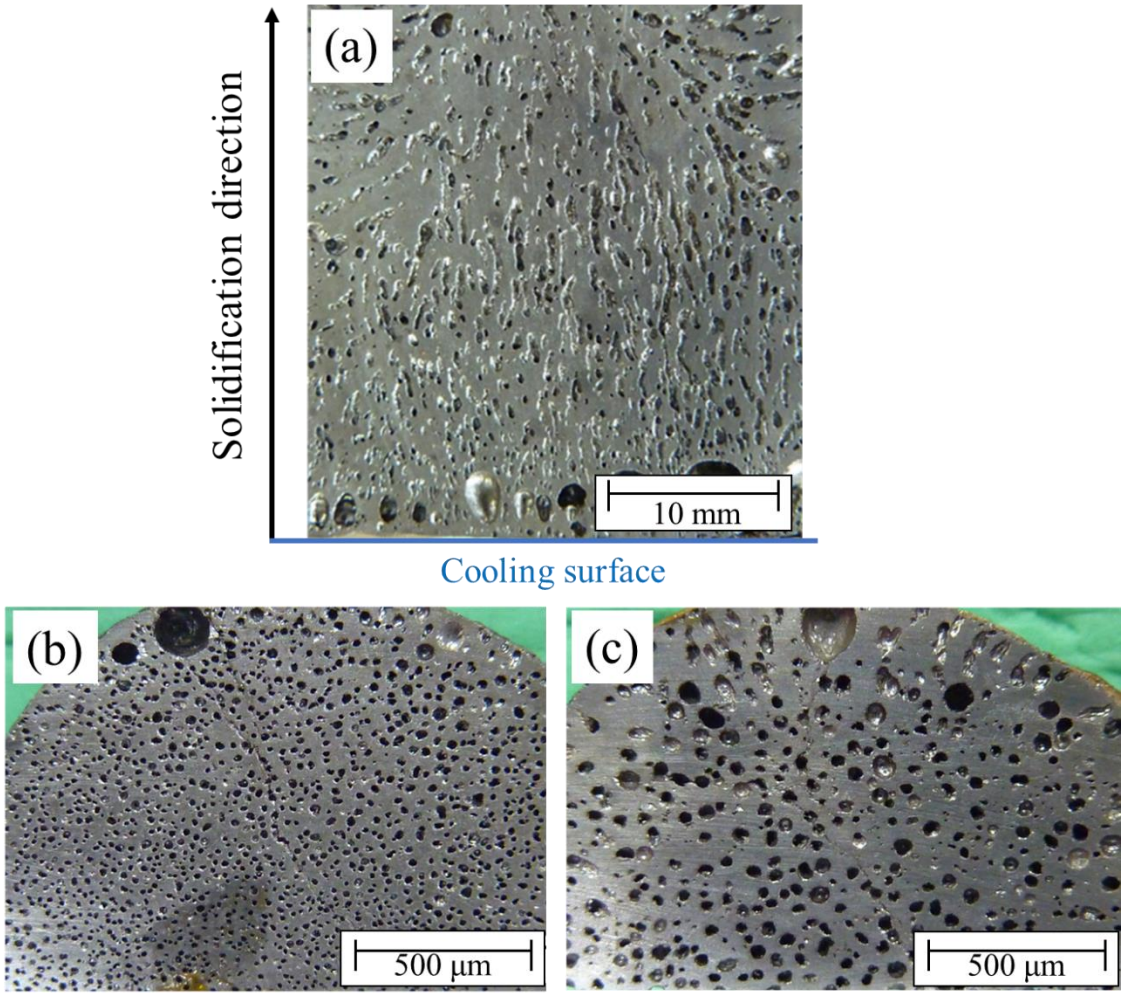

Fig. 2-2. Parallel and vertical cross section of porous Si-1at. % B samples (H2, 0.3 MPa) (a) Parallel cross section. (b) Vertical cross section, 4 mm distance from cooling surface, (c) Vertical cross section, 12 mm distance from cooling surface.

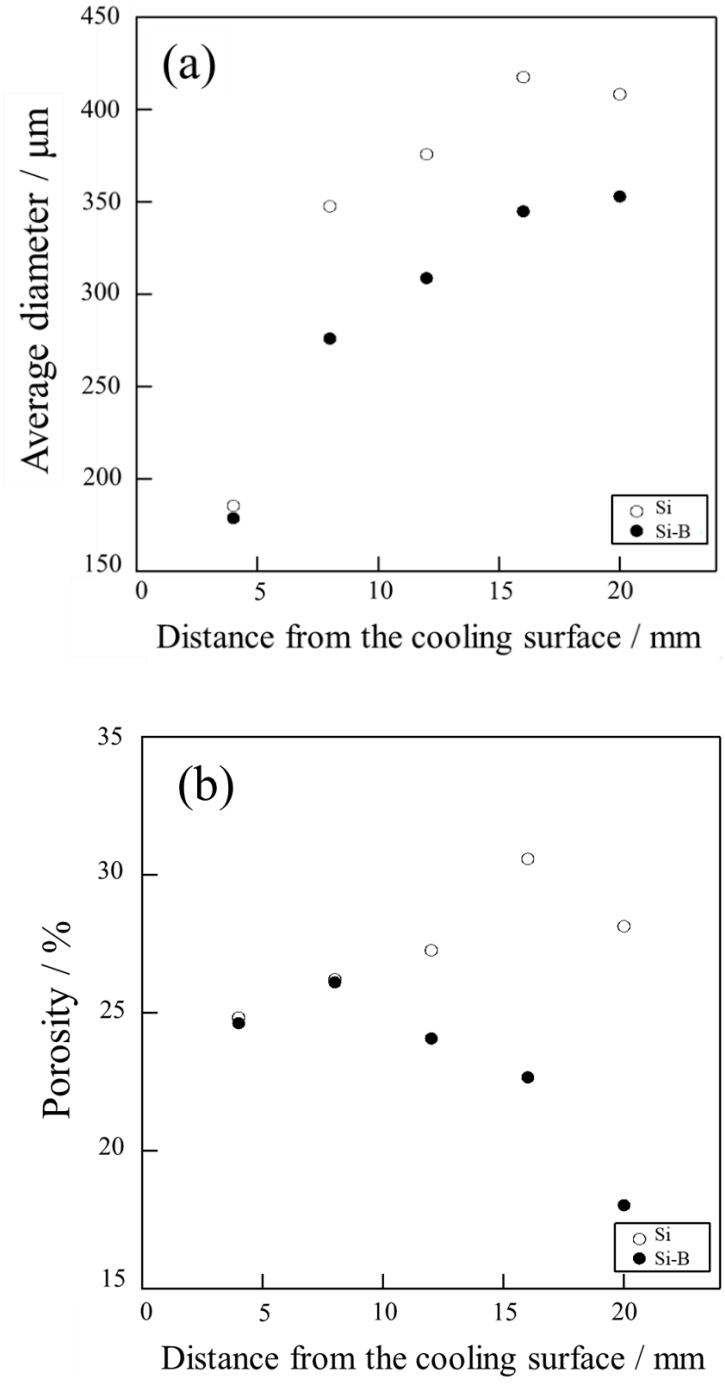

Fig. 2-3. (a) Relationship between the distance from the cooling surface and the average diameter of the pores, (b) Relationship between the distance from the cooling surface and the porosity.

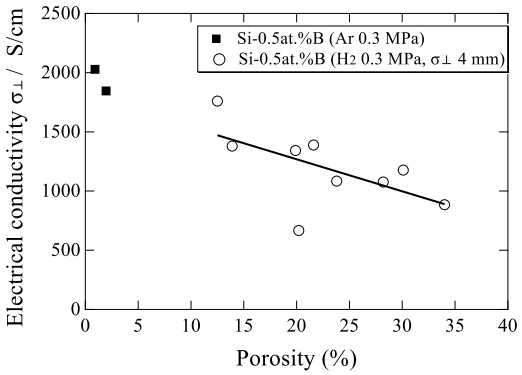

Fig. 2-4. Relationship between the electrical conductivity and porosity of porous Si-0.5at. %B (Ar/H_2 gas) perpendicular to the pores

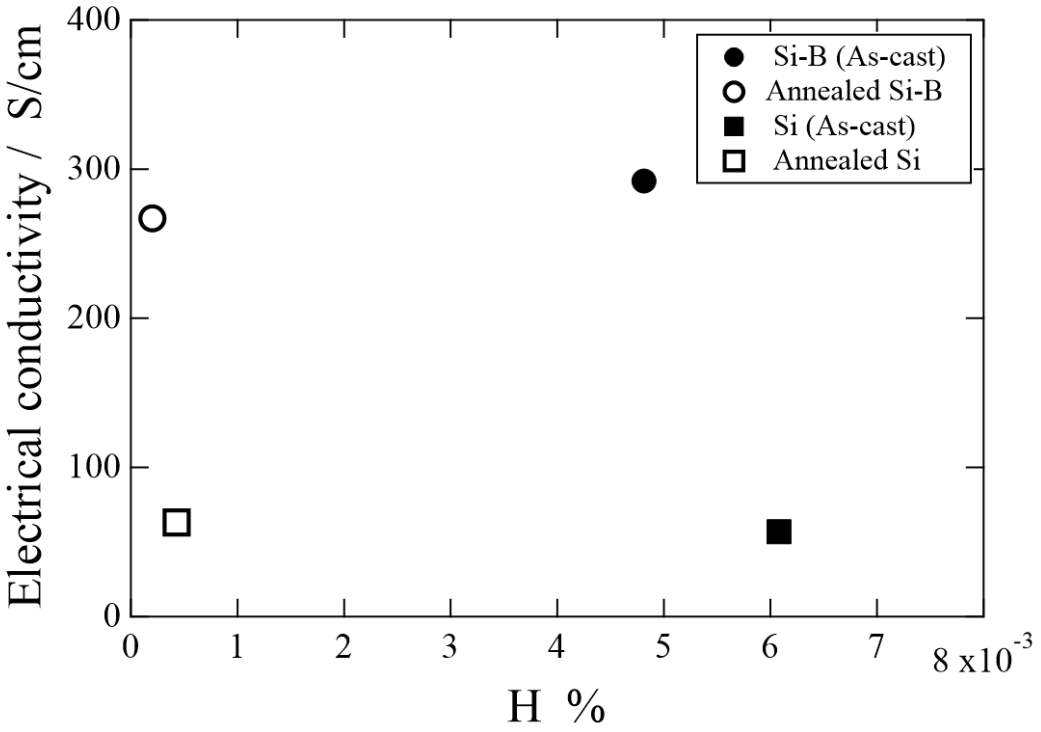

Fig. 2-5. Relationship between the hydrogen concentration and the electrical conductivity.

3. Bonding of Si to metal electrodes

In order to fabricate thermoelectric conversion devices, the bonding of thermoelectric material and metal electrode is essential. In particular, silver (Ag) is one of candidates for metal electrodes because of its high electrical conductivity and the absence of intermediate compounds with Si [13, 14]. The bonding properties between Si and Ag at the atomic scale and the shear strength have been reported in the past. [15-18]. However, more data such as bonding strength and contact resistance are needed for fabrication of thermoelectric devices using porous Si and their use. The present study investigates the diffusion bonding between Si and Ag. The strength of a joint and interfacial electrical resistivity have been evaluated.

3-1. Experimental procedure

Bonding between Si and Ag were executed using a diffusion bonding technique. A schematic diagram of the diffusion bonding is shown in Fig. 3-1. For preparation of Si/Ag diffusion-bonded samples, phosphorus-doped Si (carrier density 2.69×10^{18} cm^{-3}, 11.5 mm thick) and Ag sheet (99.998% purity, 0.5 mm thick) were used. A Si chunk was cut into a rectangular parallelepiped with an approximately 7 mm × 7 mm. square section by a wire electric discharge machine (HS-300, Brother Industries, Ltd.). The surface of the Si sample that was going to be bonded was grinded using a series of sandpapers and was polished finally with diamond slurry solution (9 μm and then 1 μm) on a plastic-metal composite disc. Ag sheet was cut into a square shape with 7 mm on a side. The Si and Ag samples were placed in a carbon die with a 27 mm diameter hole. Diffusion bonding was performed under a uniaxial pressure (SPD4000-I, Dai-ichi Kiden Co.,Ltd.) at a high temperature in an Ar atmosphere. Table 1 shows the detailed conditions used in the bonding process.

The diffusion-bonded samples were then subject to strength of a joint measurements followed by fracture surface observations and electrical resistance measurements.

For tensile tests, a stainless-steel ring was attached to each end member of diffusion bonded samples using a high-strength adhesive. Stainless steel wires were threaded through the ring, pulled at a rate of 1 $mm\cdot min^{-1}$ in a tensile tester (Instron Model 4400

Universal Testing Systems, Instron Corporation) until fracture. Measurements were performed three times for each sample. Fracture strength per unit area was evaluated from the force at the fracture and the cross-sectional area of the sample, which was 7 mm × 7 mm (Fig. 3-2).

Microstructural observations were made to examine the bonding status. In order to observe the center, a diamond saw was used to cut perpendicular to the joint surface, and their surface were polished with a series of water-resistant abrasive papers, followed by alumina paste slurry and colloidal silica on a buff. The bonding interface was observed using a scanning electron microscopy (SEM, S-4800, Hitachi High-Tech Corp.). Besides, for the sample after the tensile test, the fraction of the area where Ag and Si were microscopically well-bonded were determined. 10 randomly selected Si surface bonds in the samples (30min, 120min, 180min annealed samples) were observed under a microscope using SEM. The contact area of the fracture Si surface was calculated by using image analysis software Image J (ver.1.52a, National Institutes of Health and the Laboratory for Optical and Computational Instrumentation). The fraction of the area where Ag and Si were microscopically well-bonded were determined color shading on the surface after the fracture.

The electrical resistances of bonded samples were measured using a thermoelectric measurement and evaluation system (ZEM-3, ADVANCE RIKO, Inc.). In the measurements, Ag and Si in each samples were arranged in series in the electrical circuits, where the lengths of Ag and Si are 0.5 mm silver sandwiched between 5.75 mm Si, respectively. Samples were cut into rectangular parallelpiped with cross sections of 3 mm × 3 mm squares using a wire electric discharge machine. The resistivity of Si and Ag which were also used in the diffusion-bonded samples were measured to evaluate the interface resistances of diffusion-bonded samples. The same sample was measured a total of six times while inverting the top and bottom.

3-2. Results and discussions

3-2-1. Evaluation of strength of a joint

Result of tensile tests are shown in Fig. 3-3. The strength of a joint[1] is shown for various sample preparation conditions as functions of annealing time. The data points include either the fracture strength at the Si/Ag bonding interface or the fracture strength for cases where fracture occurred originating with cracking in Si. The error bars shown for the points for 10 MPa slow cooling mean two standard deviations from the mean values. The error bars for other conditions are not shown since their range of errors are not very different from those for 10 MPa slow cooling. It is found that the strength of a joint increases as the bonding time increases until 90 min for all bonding pressures while it does not vary significantly after 90 min. It is also found that higher bonding pressure (20 MPa) gives higher strength of a joint than lower bonding pressure (10 MPa). In addition, the strength of a joint is higher for the slow cooling (10 $K \cdot min^{-1}$) than for the air cooling (~15 $K \cdot min^{-1}$ in average).

Si fracture surfaces after tensile tests are shown in Fig. 3-4. For some air-cooled samples, fracture occurred in Si close to the bonding interface instead of the bonding interface. This trend is more remarkable for a long bonding time more than 120 min. The cause of the Si fracture could be attributed to the formation of cracks (Fig. 3-4 (c)) in Si caused by the internal stress due to the difference in the thermal expansion coefficients of Si (2.7×10^{-6} K^{-1}) [19] and Ag (1.9×10^{-5} K^{-1})[8, 20]. Therefore, it can be presumed that samples that fractured from the crack have a higher bonding strength at the bonding interface than the strength of a joint obtained in this study. In order to prevent the fracture due to the cracks, it is necessary to relieve internal stress by performing diffusion bonding at lower temperatures or slow cooling right after diffusion bonding [21, 22]. Actually, it is found in Figs 3-3 and 3-4 that slowly cooled samples exhibit higher strength than air-cooled samples and tend to fracture at the bonding interface.

Recent studies suggest that porous Si, which has higher specific surface area, shows an increased effective heat transfer coefficient, which could compensate for a disadvantage

---

[1] Strength of a joint here refers to the apparent fracture strength of the bonded samples in tensile tests.

of the high thermal conductivity of Si for application for thermoelectric conversion devices [6, 9, 23]. Such devices could be used for waste heat recovery utilizing hot wastewater from industry or hot springs. Regarding to this type of devices, the bonding strength between porous Si plates and metallic electrodes presumably need to withstand water pressure. The water pressure standard for industrial water supply in Japan is considered to be at most 0.5 MPa [24]. The results of the present work shows that the strength of a joint is high enough to withstand water pressure. It should be mentioned, however, that further studies are desired for more detailed distribution of stresses due to water pressure, difference in thermal expansion coefficients of Si/metallic electrodes and Si/thermal insulating materials.

3-2-2. Observations of bonded and fracture surfaces

SEM images of the interface between Si and Ag (10 MPa pressure, bonding time 120 min, slow cooling) are shown in Fig. 3-4(a) and (b). It is found that Si and Ag were bonded uniformly. No voids are observed at the interface. Small bumps of Ag (~ 3 μm) are observed sticking into Si. These are thought to be formed by plastic flow of Ag into the scratches of Si formed in the preparation of Si surfaces by polishing. There are no compounds formed at the interface between Si and Ag, which is consistent with the reported phase diagram [13].

Macroscopic appearances and microstructures of the fracture surface on the Si side of the sample that fractured at the bonding interface by tensile tests (10 MPa pressure, bonding time 30, 120, 180 min, slow cooling) are shown in Fig. 3-4(c). The dark phase in the SEM images is Si and the bright phase is Ag remaining on the surface of Si. Here, the area fraction of Ag residue on the fracture surface was evaluated by image analysis on the SEM images using an Image J software as shown in Table 3-2. It is found that the Ag residue on the fracture surface increases with increasing bonding time until 180 min. while, the increase from 120 to 180 minutes was small (about 3%), suggesting that the bonding strength at the interface is close to its upper limit. There is a trend that the bonding strength increases with increasing the area fraction of Ag residue. From this result, it is likely that the Ag residue is formed because the bonding between Ag and Si is strong and hence Ag is fractured in such regions. On the other hand, in the regions where Si is observed on the fracture surface, the bonding between Ag and Si is thought to be weak and Si is exposed as a result. From the fact that the fraction of Ag residue depends on bonding time, the area fraction of bonding can be controlled by bonding time.

Thus, there are factors that increases and decreases the strength of a joint: increase in bonding strength at the interface due to the increase in bonding area which is observed as the increase in the area fraction of Ag residue for longer bonding time or higher pressure, and decrease in apparent bonding strength, *i.e.* strength of a joint, due to cracking in Si, which is mention in 3-1.

3-2-3. Resistivity measurements

The results of electrical resistance measurements of Si/Ag bonded samples (10 MPa pressure, slow cooling) are shown as functions of bonding time in Fig. 3-6. The error bars mean two standard deviations from the mean value. The resistance of the bonded samples (10 MPa, 30min, slow cooling) is the same order of magnitude as the summation of resistances of Si and Ag pieces with the same dimensions as those in the bonded samples evaluated based on resistivity measurements of Si and Ag. The increase in the resistance corresponds to an interfacial resistance. There is no clear trend in the interface resistance variation with bonding time. The following equation was used as the error in interface resistance.

$$\sigma_{Interface} = \sqrt{(\sigma_{Si})^2 + (\sigma_{Bond})^2}$$

where σ_{Si} is standard deviation of Si resistance measurement, σ_{Bond} is standard deviation of Si/Ag resistance measurement. The interface resistivity is evaluated to be typically ~1.7×10^{-10} Ωm^2 (10 MPa, 30min, Average), the maximum is 5.2×10^{-9} Ωm^2 (10 MPa, 30min, $+2\sigma_{Interface}$), which is found to be about 2 times larger than those for n-type Pb-Te and Fe or Ni bonding and smaller than those for n-type Pb-Te and Al [25].

It is evident from these results that Ag is effective for Si bonding because there is no insulating layer such as an intermediate compound between Si and Ag.

3-3 Conclusions

The present work studied diffusion bonding between Si and Ag as a fundamental technology to fabricate thermoelectric modules using Si as thermoelectric material and silver as metallic electrodes. The diffusion bonding was successfully made at 1103 K under unidirectional compression load. No intermediate phase was observed consistently with the reported Ag-Si equilibrium phase diagram. The strength of a joint increases with increasing bonding time up to 90 min while it does not vary around 8 MPa with bonding time longer than 90 min for the bonding with a 20 MPa bonding pressure followed by slow cooling. Furthermore, it was found to satisfy the strength of a joint required for thermoelectric devices using porous Si. On the other hand, in this measurement, no significant variation in electrical resistance with bonding time was observed. However, the interfacial resistivity is in the order of 10^{-10} Ωm^2. Thus, Ag is useful as metallic electrodes for Si.

Table 3-1. Condition of bonding Ag and Si.

Preset Temperature [K]	1103
Bonding pressure [MPa]	10, 20
Bonding time [min]	30, 60, 90, 120, 150, 180, 300
Cooling condition [K・min^{-1}]	15 (Air cooling), 10 (Controlled cooling)

Table 3-2. Area of Ag remaining on the surface of Si calculated by Image J (10 MPa pressure, slow cooling).

Bonding time (min)	Fraction of Ag residue (%)	Strength of a joint (MPa)
30	35.58	3.38
120	55.61	6.62
180	58.54	6.22

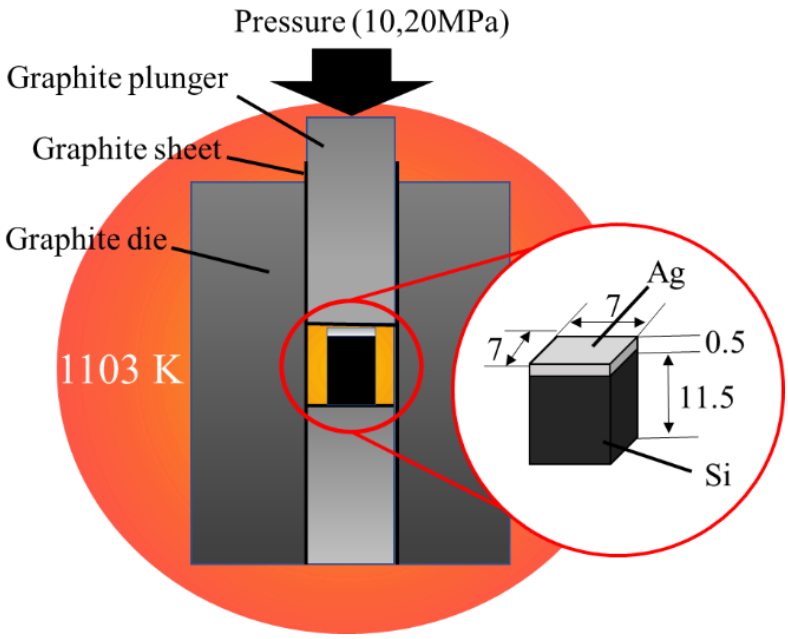

Fig. 3-1. Schematic diagram of the diffusion bonding.

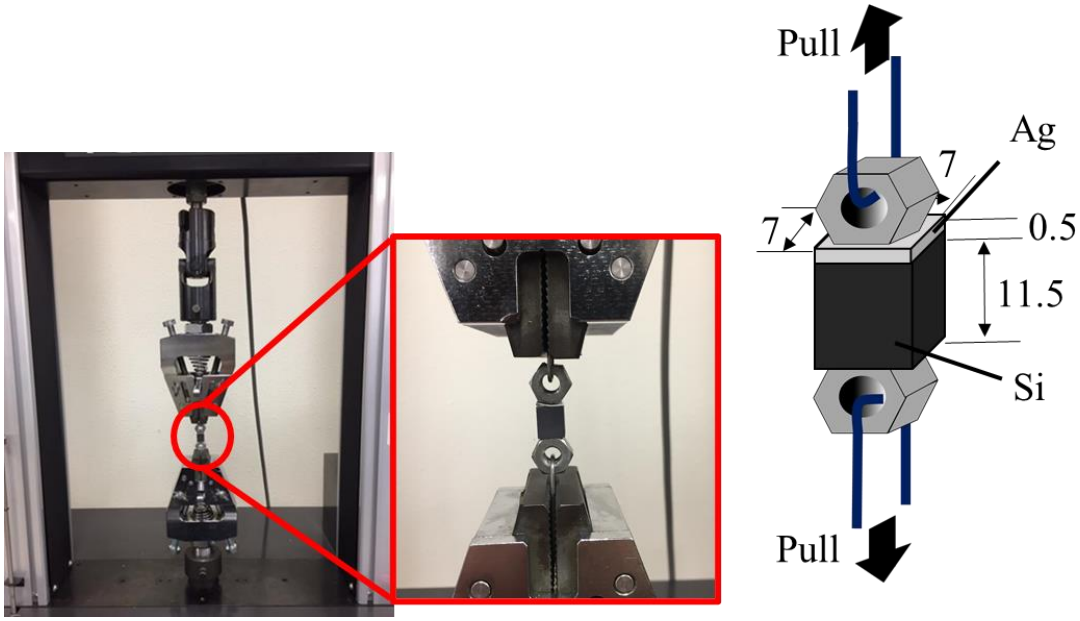

Fig. 3-2. Measurement by tensile test.

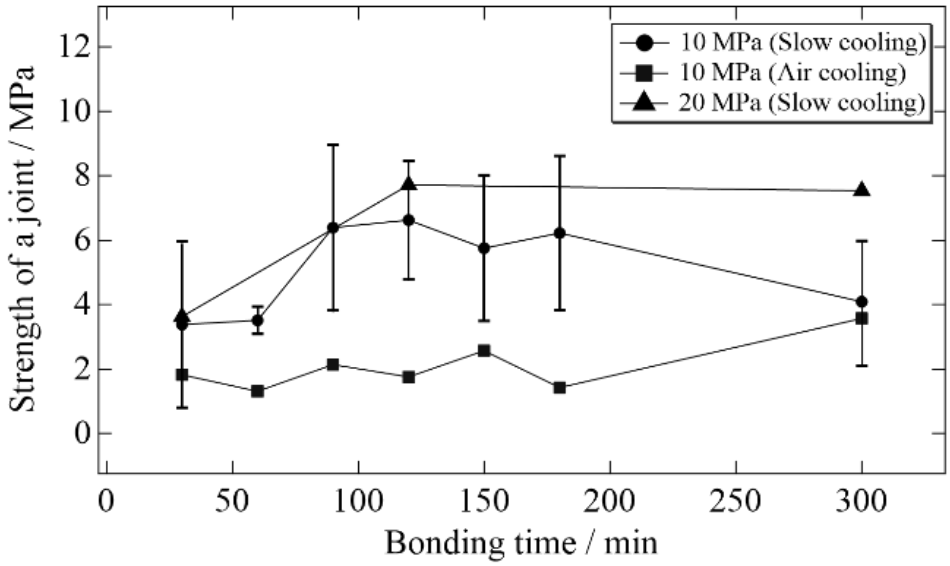

Fig. 3-3. Strength of a joint between Si and Ag under various bonding conditions shown as functions of bonding time.

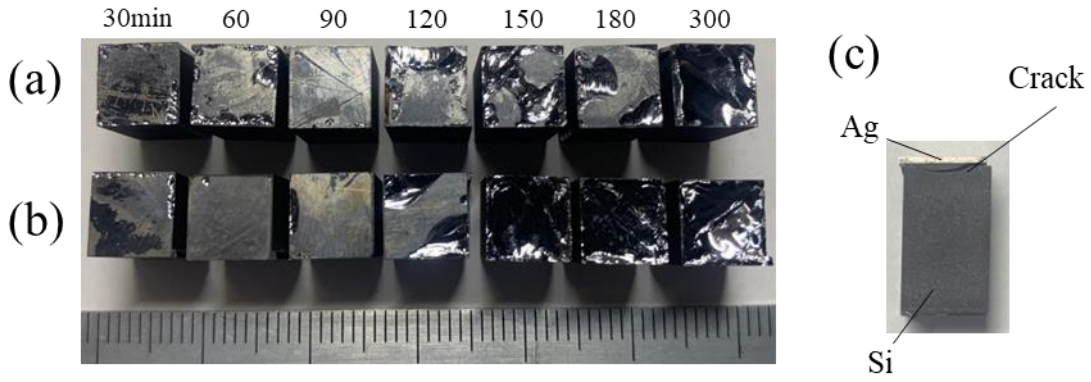

Fig. 3-4. Si fracture surfaces after tensile tests of samples prepared under (a) 10 MPa pressure and slow cooling, and (b) 10 MPa pressure and air cooling. The numbers on the top of the images indicate the bonding time. (c) A side view of a sample (prepared by 300 min bonding followed by air cooling).

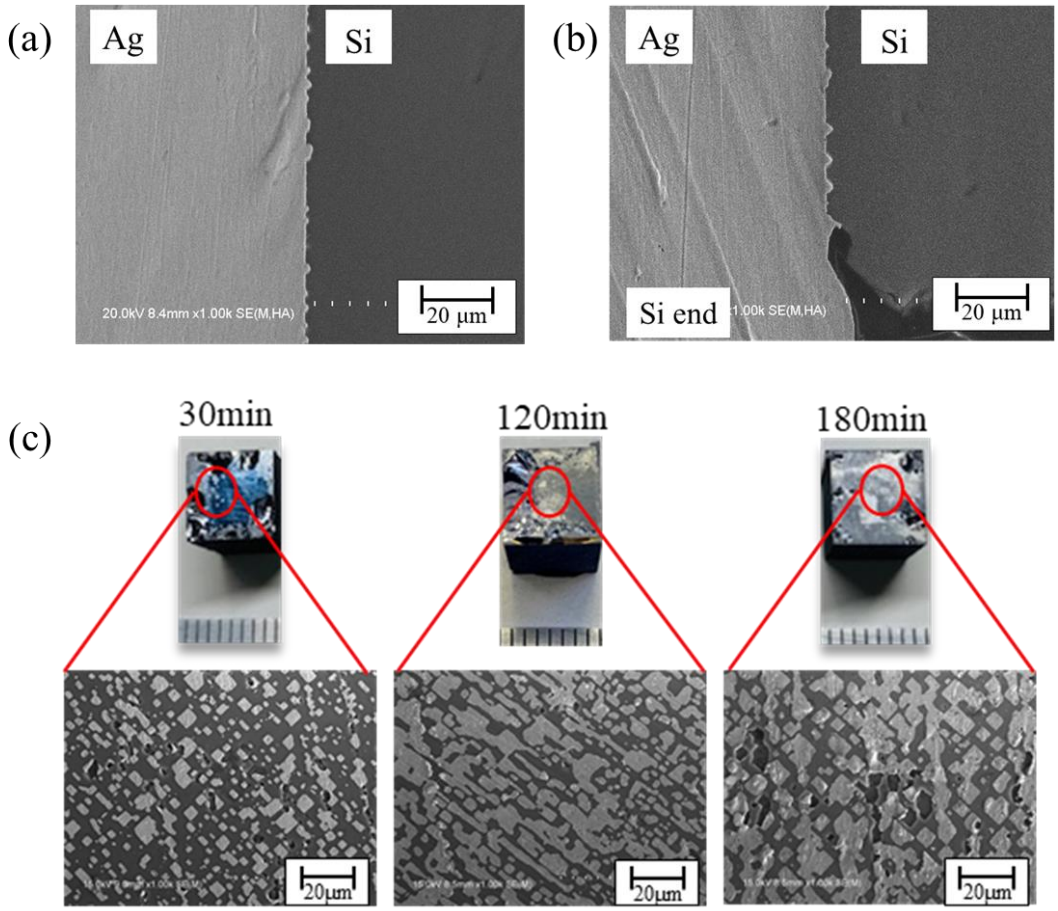

Fig. 3-5. An SEM image of the center (a) and the edge (b) of the bonding interface between Si and Ag (10 MPa pressure, bonding time 120 min). Fig. (c) shows a picture and SEM image of Si surface after tensile test (10 MPa pressure, bonding time 30, 120, 180 min).

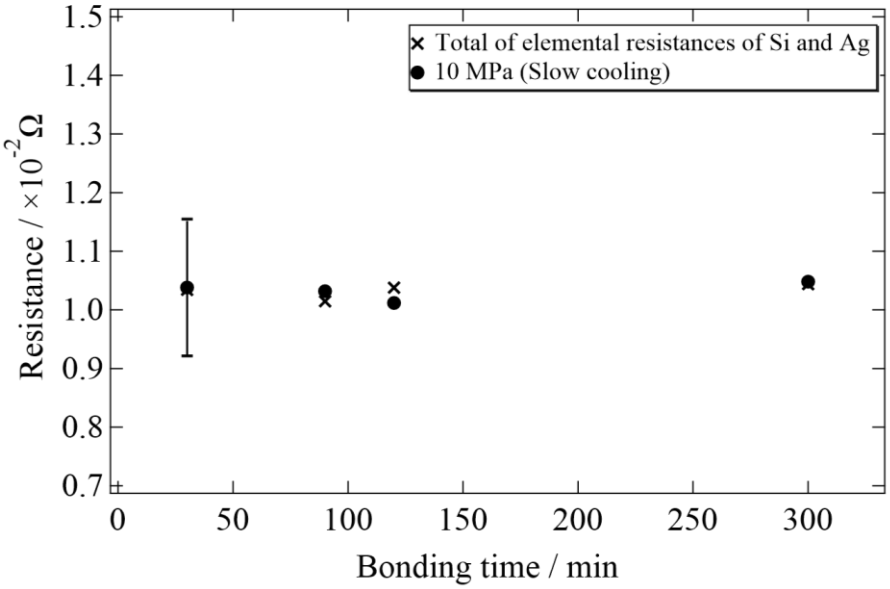

Fig. 3-6. Resistance of the Si/Ag bonded samples measured perpendicularly to the bonding interface as functions of bonding time.

4. Fabrication of porous thermoelectric conversion device

Based on the knowledge obtained in this study, we fabricated a device using porous thermoelectric materials.

4-1. Particle method simulation

To obtain design guidelines for the device, the temperature distribution of a thermal fluid flowing through a porous thermoelectric material was evaluated using particle method simulation [26]. The particle method is a method in which a continuum is represented by a finite number of particles and the behavior of the continuum is calculated by the motion of the particles. Particles are used as calculation points, and each particle moves while maintaining variables such as velocity and pressure. The particle method simulation has the following features.

- The analytical model can be easily created as particles arranged at equal intervals in the shape data.
- The positional relationship between the particles is not fixed, so it can handle large deformations.
- The free surface can be easily extracted by the position of the particles.

Therefore, the particle method is suitable for fluid analysis where tracking of free surfaces is an issue, superelastic material analysis with large deformation, and analysis of structures subject to fracture. In this study, we used the MPS (Moving Particle Simulation) method, which is a kind of particle method.

4-1-1. Condition of MPS

The simulation model is shown in Fig. 4-1. A porous plate (10.95 x 9.975 x 0.5, porosity 21.7%) was created using SOLIDWORKS 2016. The pores were aligned in an equilateral triangle of the two-dimensional close-packed structure. Two plates were placed parallel to each other, and adiabatic rubber was placed at the center and periphery of the plates to partition the fluid. The created model was used to evaluate the temperature when a warm body was flowing in the same direction using the MPS method (PROMETECH, Particleworks, ver 6.0). The conditions used in the simulation are shown in Table 4-1, and the physical properties used in the simulation are shown in Table 4-2. the physical properties of Si are those of a single crystal. The boundary between the fluid and the wall was assumed to be adiabatic. Simulations were performed with different pore sizes and the temperatures of the porous plates were compared.

4-1-2. Result of MPS method

The temperature distribution of a porous plate with different pore size at steady state are shown in Fig. 4-2. The fixed point is a quarter of the way from the edge. The results are for the backside of the fluid inlet side, and the porosity is equal. The temperature difference between the fixed points, and the calculated apparent heat transfer coefficient are shown in Table 1. It is clear that the smaller the pore size, the larger the temperature difference and the higher the heat transfer coefficient. This is due to the larger surface area and more frequent heat exchange.

The relationship between temperature and distance for a ϕ0.4 mm porous plate is shown in Fig. 4-3. The position from 5 mm to 6 mm is non-porous and the temperature gradient is represented by a straight line. Therefore, for a non-porous plate, the temperature gradient is considered to be an extension of this straight line. However, it was found that the temperature of the fluid approaches the temperature between 3 mm and 5 mm at the low temperature side and between 6 mm and 8 mm at the high temperature side. This is due to the enhancement of heat exchange by porosity, and these results prove the usefulness of porosity.

4-2. Device design

An example of device design considering high heat transfer is shown in Fig. 4-4. In this porous thermoelectric conversion device, the thermal fluid flows through the pores of the TE materials and exchanges heat. Increase in the thermal interface area is the greatest advantage. Alternately arranging porous Si-B (p-type) and Si-P (n-type) plates connected with the metallic electrodes in between (gray) and thermal insulation material (black), the flow paths for fluid are formed in a direction perpendicular to the plate. High-/low-temperature fluids alternately flow in the paths facilitate the temperature gradient within the TE materials resulting in the thermal electromotive force.

It is challenging to fabricate a device with multiple layers of Si plates, so we fabricated a device with four layers of N-type and P-type in this study.

4-3 Bonding of porous Si and Ag

The bonding of Si and Ag were executed using the diffusion bonding technique as well as chapter 3. The bonding process is shown in Fig. 4-5. N-type P-type porous Si and Ag are alternately placed in a carbon die. The spaces at both ends of the Ag are sandwiched between alumina plates. Diffusion bonding was performed under a uniaxial pressure (10 MPa) at a 1103 K in an Ar atmosphere. The alumina plates were removed after collecting the bonded samples. The appearance of the bonded sample is shown in Fig. 4-6 (a) (b), and the SEM image of the bonded surface is shown in Fig. 4-6 (c). Fig. 4-6 (a) shows that the Ag is placed at the targeted position by the alumina plate. From Figure 4-6 (c), it is clear that porous Si and Ag can be bonded as well as non-porous Si.

4-3-1 Fabrication of thermoelectric conversion devices using porous Si

As mentioned in chapter 2, we have succeeded in fabrication of lotus-type porous Si by unidirectional solidification under hydrogen atmosphere. However, we have not yet got lotus-type porous Si with pores long enough to obtain porous Si plates with a high penetration rate. Therefore, we made holes in Si plates using a drill instead. The porous Si plate fabricated by hand drilling is shown in Fig. 4-7. The devices were fabricated in a size of 17 mm × 17 mm, with one Si-B (resistivity $\rho \leq 0.02\ \Omega$ cm) and one Si-Sb ($\rho \leq 0.02\ \Omega$ cm) bonded to each other with Ag. A hole of 1.2 mm in diameter was drilled. The porosity of the Si plates are 9.38%. The reason for the diameter of 1.2 mm is that the smallest diameter of the hand drill as selected. If the distance between the holes is too close, the Si plate will crack, so the holes were drilled at the minimum distance that would prevent the plate from cracking. In the conventional porous material, the holes are randomly arranged. In contrast, in this experiment, the holes were drilled in consideration

of the position of the electrodes and the arrangement of the channels. During the bonding process, it is necessary to apply pressure below the lower limit of the high-temperature sintering equipment due to the small contact area. Therefore, metal weights were placed on top of the carbon die. Because of the limited space in the apparatus, the total weight of the weights that could be placed was 8 kg (4.8 MPa). The annealing process was carried out at 1103 K for 90 minutes under this pressure condition. Next, the bonded sample is fixed to the flow branching apparatus fabricated by the 3D printer (XYZ Printer). The design of the branching apparatus is shown in Fig. 4-8(a), and the installation is shown in Fig. 4-8(b). This device can branch the flow path in four directions. To prevent fluid leakage, the device is wrapped the tape around the device and sandwiched between insulating rubbers and fixed in the central hollow.

4-3-2 Performance of thermoelectric conversion devices using porous Si

To measure the voltage, a wire was placed perpendicular to the fluid. The end of the wire was connected to a data logger to record the time variation of the voltage. The measurement is shown in Fig. 4-9. Si tubes for hot and cold fluids were attached to the flow branch apparatus, and water was circulated by a pump (hot: 353 K, cold: 293 K). Pure water (electrical conductivity: 1×10^4 S/m) was used as the fluid. The voltage can be obtained by

$$\Delta V = S\Delta T$$

The voltages expected for one Si plates are (Si-B: about 0.5 mV/K) and (Si-Sb: about -0.4 mV/K), respectively [27-29]. Therefore, the total voltage is estimated to be about 50 mV assuming ΔT = 50 K. The relationship between time and voltage is shown in the fig. 4-10. The cold water started to flow at 25 seconds and the hot water started to flow at 47 seconds. As soon as the cold water was flowed, a temperature difference occurred in the device and the voltage was measured (9.2mV). Furthermore, when hot water was flowed, the voltage value increased and stabilized at 50-60 mV. After 70 seconds, water leakage from the device was observed, after which the voltage dropped with noise. This suggests that the temperature difference within the Si plates is not kept constant maybe due to a mixture of hot and cold water. Therefore, it is necessary to enhance the adhesion between the flow branching apparatus and the device. In this experiment, the bifurcation apparatus for the water flow and the porous Si plates were adhered only by vertical pressure via fluorine rubber. In order to achieve complete seal, adhesives or greases should be used, or the design of the bifurcation apparatus for the water flow needs to be improved further.

Table 4-1. The conditions of simulation.

Particle diameter [mm]	0.075
Flow velocity [m/s]	0.1
Temperature of hot fluid [K]	353
Temperature of cold fluid [K]	283

Table 4-2. Physical properties used in the simulation.

	ρ [kg m^{-3}]	C_p [J kg^{-1}K^{-1}]	κ [W m^{-1}K^{-1}]	ν [$\times 10^6$ m^{2}s^{-1}]
Si	2330	713.0	148.0	-
Thermal insulation	950.0	1500	0.228	-
Hot fluid	999.7	4190	0.578	1.306
Cold fluid	971.8	4200	0.669	0.365

Table 4-3. Simulation results of temperature difference between fixed points and calculated apparent heat transfer coefficient.

Pore size Φ [mm]	Temperature difference ΔT [K]	Heat transfer coefficient h [W m^{-2} K^{-1}]
2.8	37.1	8.10×10^4
0.4	63.6	3.19×10^5

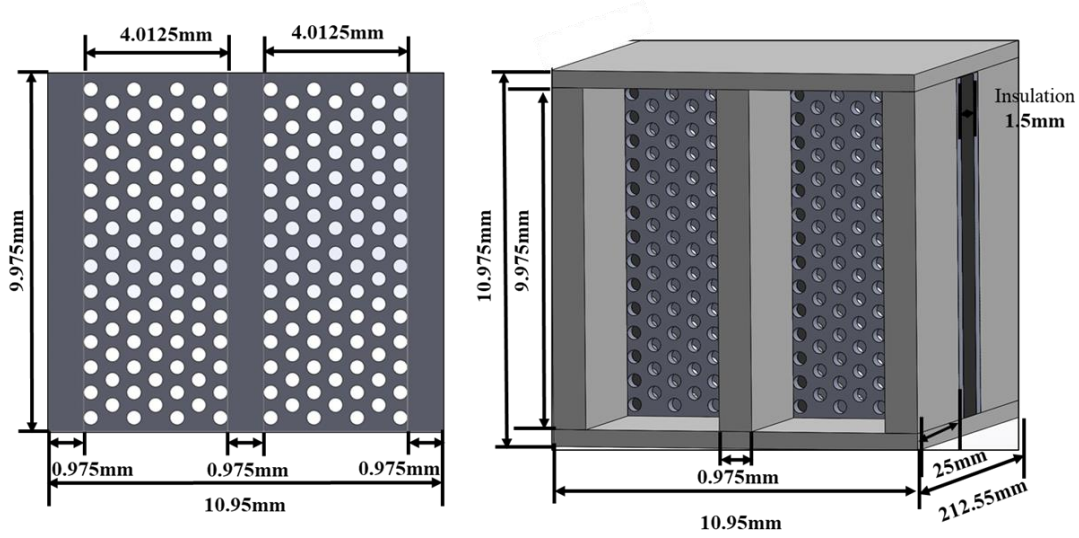

Fig. 4-1. Simulation models of MPS method.

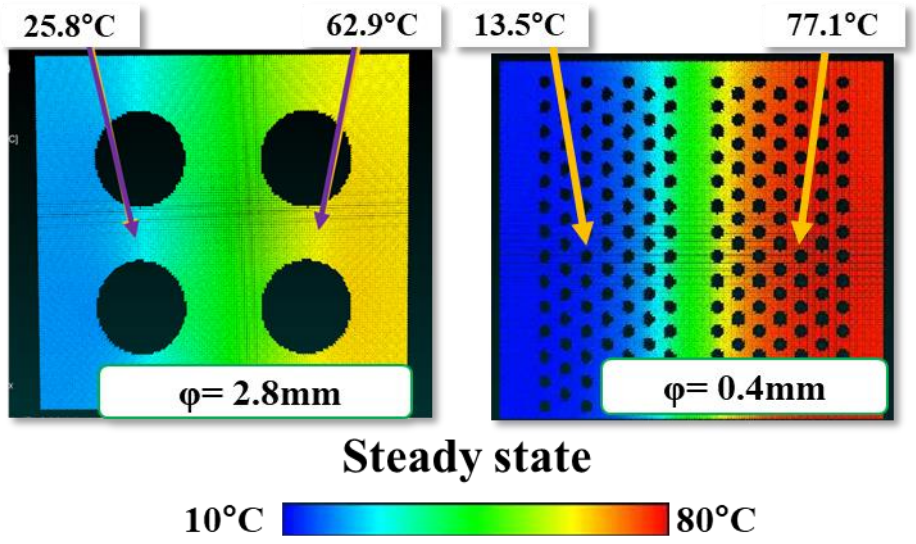

Fig. 4-2. Simulation results of the temperature distribution of a porous plate with different pore size at steady state.

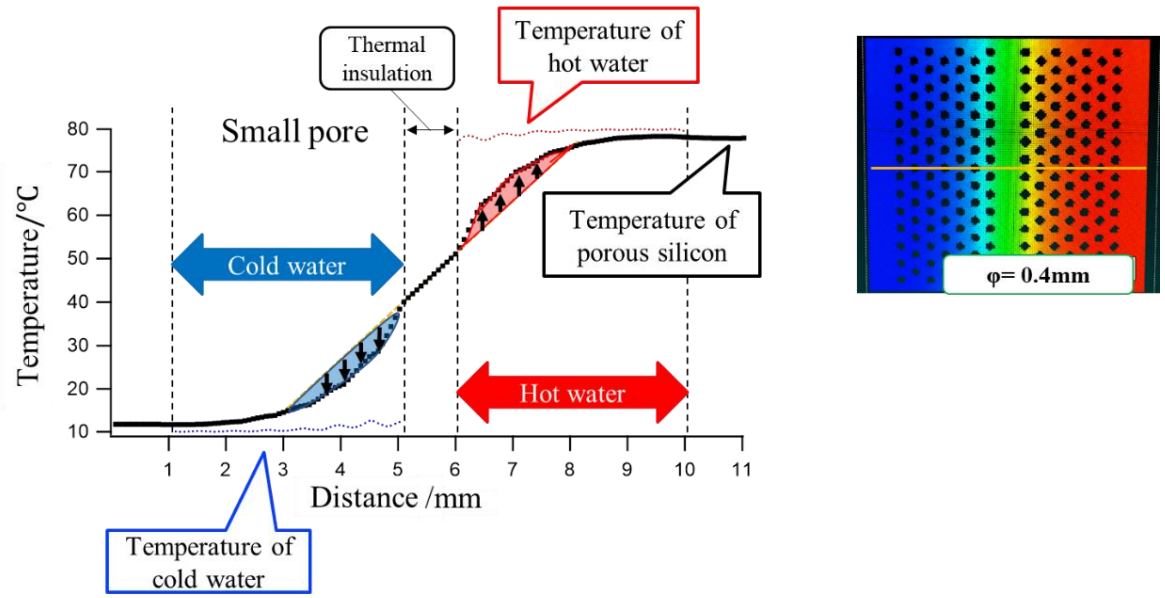

Fig. 4-3. Simulation results of the relationship between temperature and distance for a ϕ 0.4 mm porous plate.

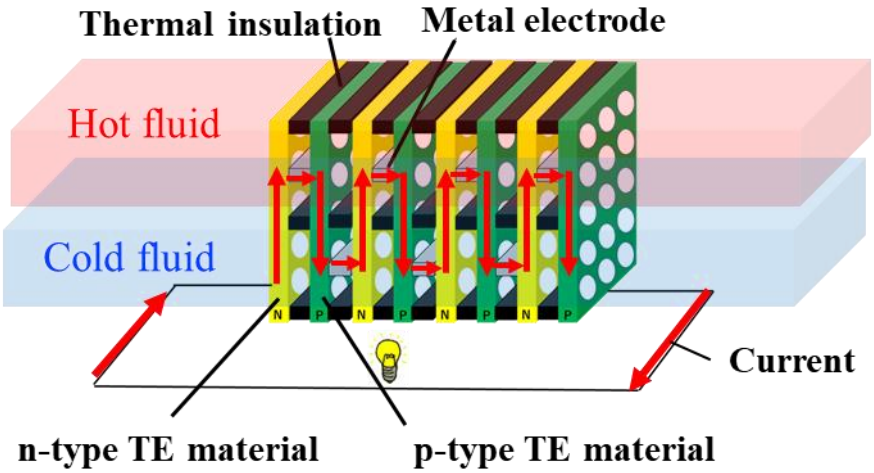

Fig. 4-4. An example of a design for a thermoelectric conversion device using a porous material.

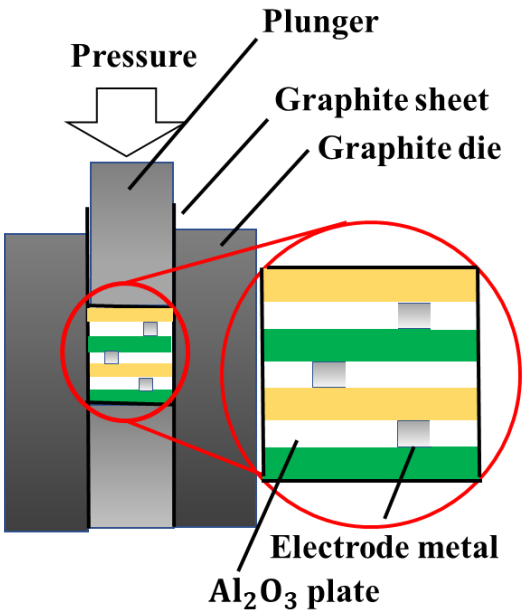

Fig. 4-5. Schematic diagram of the bonding process between Si plate and Ag.

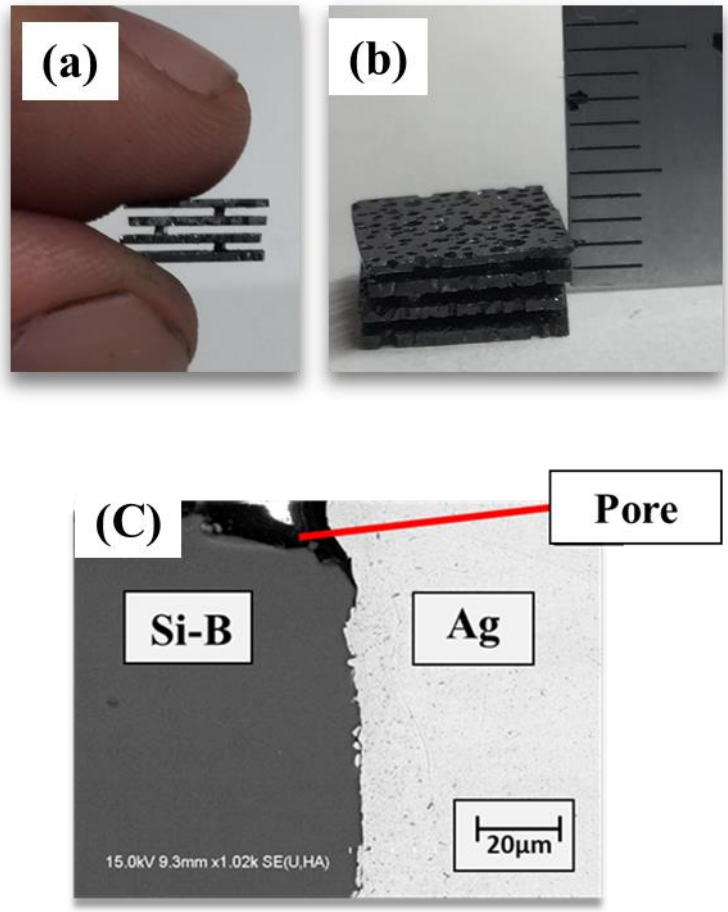

Fig. 4-6. Porous device after bonding (a) Side view (b) Overall view (c) SEM image of the bonded interface.

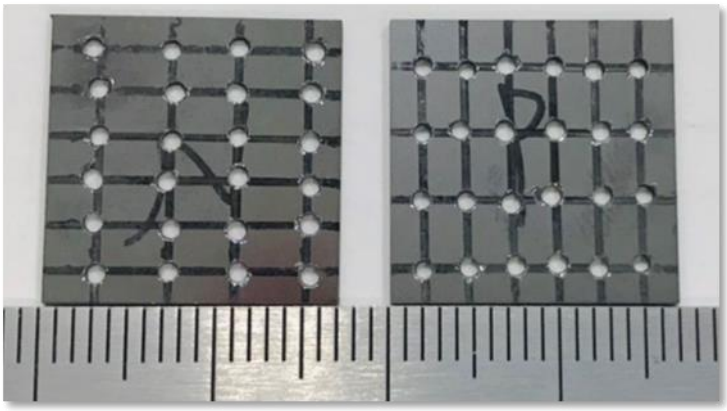

Fig. 4-7. Si plates with holes drilled by hand drill.

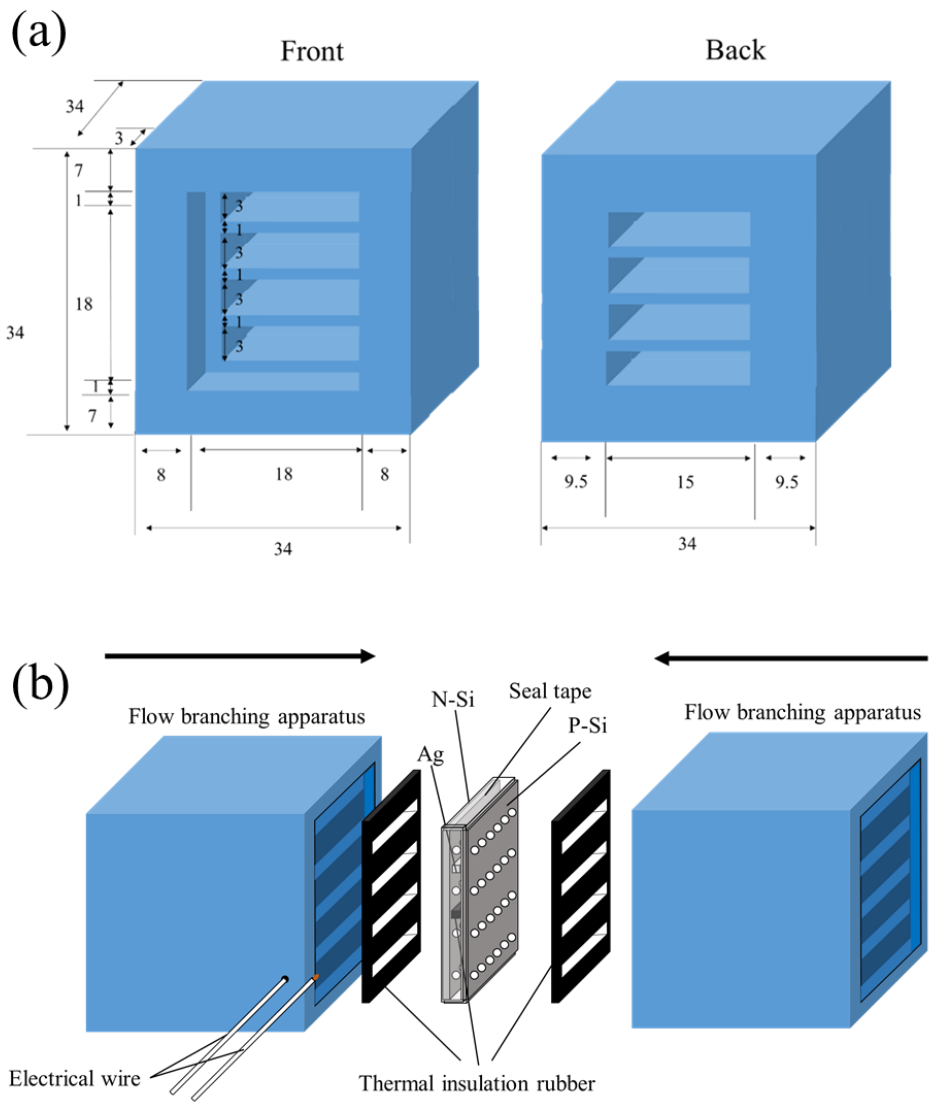

Fig. 4-8. Schematic diagram of flow branching apparatus (a)design, (b) the installation.

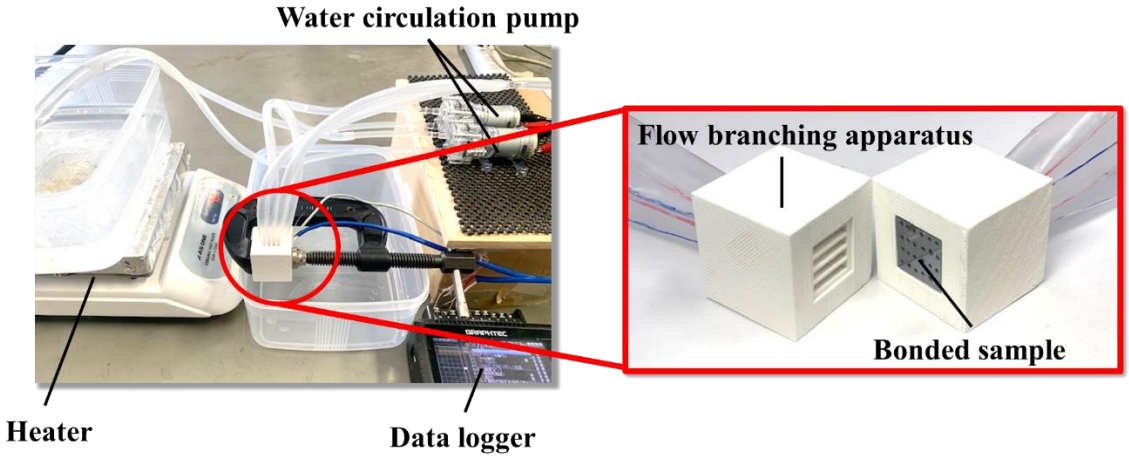

Fig. 4-9. Overall view of the voltage measurement device.

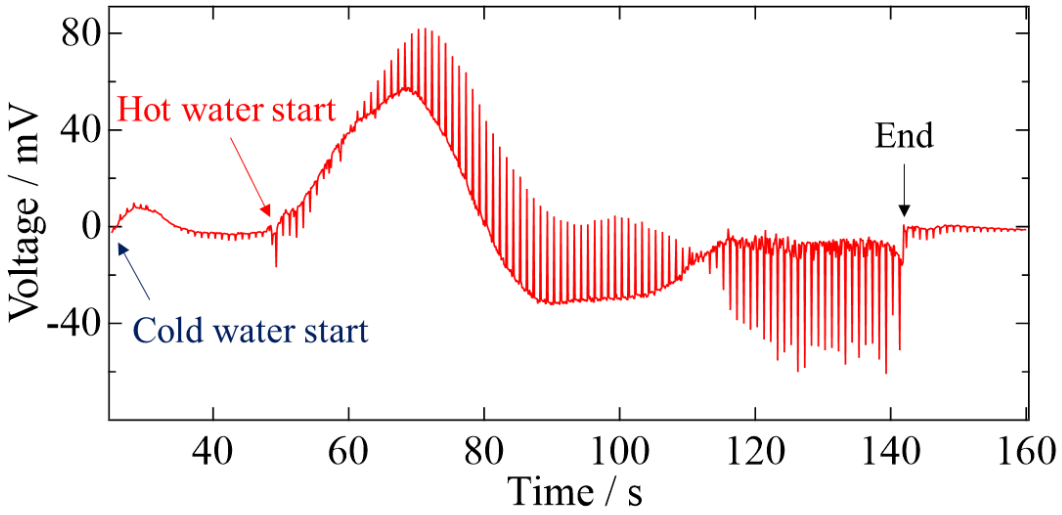

Fig. 4-9. Relationship between time and voltage in porous Si ((hot water: 353 K, cold: 293 K).

5. Conclusion

The present study investigates the fabrication of high heat transfer type thermoelectric conversion devices using porous Si.

First, fabrication of porous Si and Si-B by unidirectional solidification under hydrogen atmosphere was conducted. In addition, the influence of doping elements for tuning carrier concentration on the pore formation and the influence of hydrogen dissolved in the Si crystal on the electric properties were examined. As a result, it was found that porous Si-B with unidirectional pores can be produced by unidirectional solidification under a hydrogen atmosphere. The average diameter of pores and the porosity increase with increasing the distance from the cooling surface. It is found that the effect of B-doping on pore formation is not significant. Furthermore, it was confirmed that the residual hydrogen in porous Si and Si-B can be decreased by annealing process with vacuum evacuation. Regarding the relationship between electrical conductivity and porosity, the electrical conductivity decreases in the direction perpendicular to the porosity as the porosity increases.

Second, the bonding conditions of porous Si and Ag are examined. Diffusion bonding of Si and Ag was performed and the bonding strength and electrical resistivity were measured. Diffusion bonding was performed under a uniaxial pressure (10, 20 MPa) at 1103 K in an argon atmosphere and bonding status was observed using a scanning electron microscope. It was found that the strength of a joint increases as the bonding time increases until 90 min for both the bonding pressures. There is no clear trend in resistivity variation with bonding time. In addition, The interfacial electrical resistivity is in the order of 10^{-10} Ωm^2 and there is no significant variation with bonding time. Ag is a good candidate for an electrode material for Si because it is bonded to Si well and there is no insulating layer formed such as an intermediate compound.

Finally, porous Si devices were fabricated. Alternately arranging porous p-type and n-type Si connected with the electrodes in between and thermal insulation material, the flow paths are formed in a direction perpendicular to the plate. High-/low-temperature fluids alternately flows in the path and causes the thermal electromotive force. Hand-drilled Si wafers were used as the porous Si. The devices were fabricated in a size of 17 mm × 17 mm, with one Si-B and one Si-Sb bonded to each other with Si. Hot (about 353 K) and cold (about 293 K) temperature fluids flowed through the device, and electrical voltages of an order of mV were obtained.

While the present study has clarified the above, there are many issues to be addressed in establishing porous thermoelectric conversion devices. In order to fabricate porous

thermoelectric conversion devices, it is necessary to fabricate uniform porous thermoelectric materials with long pores and optimize the device design. To obtain thermoelectric materials with long through-pores, our group is investigating the fabrication by unidirectional solidification instead of the mold casting method and that is in the process of optimizing the solidification speed and the amount of hydrogen gas. Porous thermoelectric materials with pores extending in one direction will be realized soon. For the device design, we have to optimize the number of layers of N and P type, location and thickness of electrodes, porosity, thermoelectric properties, and fluid flow and its flow rate. In addition, we have to take into account the strength of porous thermoelectric materials. While there are many issues to be solved to realize porous thermoelectric devices, it has the potential to break through the current sluggish growth of practical application of thermoelectric devices. It is hoped that the findings that have been presented in this paper will contribute to a better understanding of the future of porous thermoelectric conversion devices.

REFERENCES

1. C. Forman, I. K. Muritala, R. Pardemann and B. Meyer, *Renewable and Sustainable Energy Reviews*, 2016, **57**, 1568-1579.
2. S. Kaminaga, *Sensors and Materials*, 2018, **30**, 723-731.
3. G. J. Snyder and E. S. Toberer, *Nature Materials*, 2008, **7**, 105-114.
4. Teruyuki Ikeda, Makoto Sasaki and Takatoshi Nagano, *Clean Energy TECHNICAL REPORT*, 2020, **29**, 51-55.
5. R. Echigo, *Journal of the Society of Mechanical Engineers*, 1993, **96**, 204-209.
6. H. Nakajima, *Proc. Jpn. Acad.*, 2010, **86B**, 884-899.
7. H. C. T. Ogushia, H. Nakajima and T. Ikeda, *JOURNAL OF APPLIED PHYSICS*, 2004, **95**, 5843-5847.
8. T. O. Hiroshi CHIBA, Hideo NAKAJIMA, Teruyuki IKEDA, *JSME International Journal* 2004, **47**, 516-521.
9. T. Nakahata and H. Nakajima, *Materials Science and Engineering: A*, 2004, **384**, 373-376.
10. Sabah K. Bux, R. G. Blair, P. K. Gogna, H. Lee, G. Chen, M. S. Dresselhaus, R. B. Kaner and J. P. Fleurial, *Advanced Functional Materials*, 2009, **19**, 2445-2452.
11. T. K. T. Ikeda, T. Nagano, T. Ide, M. Murakami, T. Numata, H. Nakajima, *Japan patent JP 2019-165137A*.
12. O. Bierwagen, R. Pomraenke, S. Eilers and W. T. Masselink, *Physical Review B*, 2004, **70**.
13. R. W. Olesinski and G. J. Abbaschian, in *Binary Alloy Phase Diagrams, II Ed*, ed. T. B. Massalski, ASM international, 1990.
14. R. A. Matula, *Journal of Physical and Chemical Reference Data*, 1979, **8**, 1147-1298.
15. S. Jay Chey, L. Huang and J. H. Weaver, *PHYSICAL REVIEW B*, 1998, **59**, 33-41.
16. J. Li, C. M. Johnson, C. Buttay, W. Sabbah and S. Azzopardi, *Journal of Materials Processing Technology*, 2015, **215**, 299-308.
17. Tomoki MATSUDA, Kota INAMI, Keita MOTOYAMA, Tomokazu SANO and A. HIROSE, *Smart Processing Society of Materials, Environment and Energy*, 2019, **8**, 177-183.
18. P. J. Wang and C. C. Lee, *in IEEE Transactions on Components and Packaging Technologies*, 2010, **33**, 10-15.
19. Hiromichi Watanabe, Naofumi Yamada and Masahiro Okaji, *International Journal of Thermophysics*, 2004, **25**, 221-236.
20. Y. S. Touloukian, R. K. Kirby, R. E. Taylor and P. D. Desai, *Thermal Expansionn-metallic elements and alloys*, IFI/Plenum, 1975.
21. Mitsuhiko KIMURA, Koichi ASARI, Shoji GOTO and S. ASO, *Quarterly Journal of the JWS*, 2003, **21**, 448-459.

22. Naoto SHIRAKI, Y. SUGIYAMA and K. MINO, *J. Soc. Mat. Sci., Japan*, 2001, **50**, 1120-1125.
23. Teruyuki Ikeda, Makoto Sasaki and T. Nagano, *Clean Energy TECHNICAL REPORT*, 2020, **29**, 10-15.
24. *Journal of industrial water*, 2014, **626**, 55-61.
25. Y. Hori, *Central Research Institute of Electric Power Industry report*, 2002, **W01006**, 01-03.
26. M. Fumikazu, *Journal of The Japan Welding Society*, 2011, **80**, 534-537.
27. J. Sadhu, H. Tian, J. Ma, B. Azeredo, J. Kim, K. Balasundaram, C. Zhang, X. Li, P. M. Ferreira and S. Sinha, *Nano Lett*, 2015, **15**, 3159-3165.
28. K. Valalaki, P. Benech and A. Galiouna Nassiopoulou, *Nanoscale Res Lett*, 2016, **11**, 201.
29. A. Yusufu, K. Kurosaki, Y. Miyazaki, M. Ishimaru, A. Kosuga, Y. Ohishi, H. Muta and S. Yamanaka, *Nanoscale*, 2014, **6**, 13921-13927.

Acknowledgments

I would like to express my sincere gratitude ~~and appreciation~~ to my supervisor, Prof. Teruyuki Ikeda, for all his constructive supervision and invaluable guidance throughout my PhD research.

I would like to thank our collaborator, Dr. Takatoshi Nagano at Ibaraki University and Dr. Takuya Ide at Lotus Thermal Solution Inc. for their helpful measurements and comments that ~~provide~~ lead to better understanding in my research.

My heartfelt appreciation goes to Prof. Chihiro Iwamoto ~~at Ibaraki University~~ and Prof. Yasushi Sasajima at Ibaraki University and Assoc. ~~prof~~Prof. Masakazu Tane at Osaka University whose comments and suggestions were of inestimable value for this~~my~~ study.

I would like to thank Prof. Haruhiko Udono and his group members in Department of Electrical and Electronic Systems E~~e~~ngineering ~~Department~~ at Ibaraki University, who~~to~~ kindly g~~a~~ive us~~me~~ the opportunity to measure the electrical and thermal properties of our~~my~~ samples. And I would like to thank Dr. Nagano's group members for their kind help in the fabrication of the cases of thermoelectric conversion devices using a 3D printer.

I really appreciate all my colleagues in the Prof. Ikeda's group, especially Mr. Takahumi Kojima, Takuya Yamazaki, Makoto Sasaki, Yohei Hiyama and Yutaro Abematsu for their kind help and support. In addition, thanks to Dr. Babak Alinejad, Yuta Aoki, Yuma Yamamoto, Hiroki Matsui, Ryuta Yurishima, Syunsuke Sumi, Seiya Nakayama, Kaito Yamakawa, and Ms. Mamiko Kimura in the Ikeda Laboratory, I was able to have a very enjoyable and meaningful research life.

Finally, I would also like to express my gratitude to my family for their support and warm encouragement.

I hope you have a great success in your future.